PHYSICAL REVIEW C **89**, 011306(R) (2014)

First characterization of *sd*-shell nuclei with a multiconfiguration approach

J. Le Bloas,[1] N. Pillet,[1] M. Dupuis,[1] J. M. Daugas,[1] L. M. Robledo,[2] C. Robin,[1] and V. G. Zelevinsky[3]
[1]*CEA, DAM, DIF, F-91297 Arpajon, France*
[2]*Universitad autonoma de Madrid, Madrid, Spain*
[3]*Department of Physics and Astronomy and National Superconducting Cyclotron Laboratory, Michigan State University, East Lansing, Michigan 48824, USA*
(Received 1 August 2013; published 30 January 2014)

In this work, we propose a new description of nuclear spectroscopy based on the analysis of a rather complete set of observables, using the multiparticle-multihole configuration mixing and the D1S Gogny interaction. The application to the even-even *sd*-shell nuclei, for both ground and 0_2^+, 1_1^+, 2_1^+, 2_2^+, 3_1^+, 3_2^+, 4_1^+ excited states, clearly shows the pertinence of this approach. The standard deviation to experiment is ∼500 keV for two-nucleon separation energies and ∼400 keV for excitation energies. The calculated magnetic dipole moments and $B(M1)$ transition probabilities are in a very good agreement with experiment. Concerning the spectroscopic quadrupole moments and $B(E2)$ transition probabilities, the experimental trends are systematically reproduced. Only a lack of quadrupole collectivity appears. A solution to improve this expected defect is suggested.

DOI: 10.1103/PhysRevC.89.011306 PACS number(s): 21.60.Jz, 21.10.Ky, 21.60.Cs, 23.20.Lv

Introduction. In nuclear physics, the mean-field (MF) type [1–13] and the shell-model (SM) [14–16] methods are the two most common and powerful approaches to the many-body problem. The MF approaches are based on approximate self-consistent solutions using the symmetry breaking/restoration and implying all the nucleons. They are almost applicable to the whole chart of nuclei being effective predominantly for the description of ground states. Conversely, the SM solution preserves the symmetries of the nuclear Hamiltonian, allowing a natural contribution of all types of correlations and describing spectroscopic observables. However, an inert core plus valence particles decomposition is assumed, reducing its domain of applicability.

Following the old dream of the *unified model* of Bohr and Mottelson in order to reunify the two pictures, and keeping their specific advantages (self-consistency, symmetry preservation, etc.), we have recently proposed a multiconfiguration description of the many-body systems [17,18], using the D1S Gogny interaction [24]. In the present work, we investigate for the first time the ground- and excited-state energies as well as the magnetic dipole and electric quadrupole collectivities of the 25 even-even *sd*-shell nuclei [$8 < (N,Z) < 20$] using the newly proposed *m*p-*m*h configuration mixing (CM) approach. The analysis is done in the same spirit as previous MF and SM studies [19–23].

The multiparticle-multihole (*m*p-*m*h) configuration mixing (CM) constructs an energy density functional $\mathcal{F}(\rho)$ with a trial wave function $|\Psi\rangle$ corresponding to a superposition of Slater determinants built as multiple particle-hole (p-h) excitations on this reference state:

$$\mathcal{F}(\rho) = \langle\Psi|\hat{H}(\rho)|\Psi\rangle - \lambda\langle\Psi|\Psi\rangle - \sum_i \lambda_i Q_i, \qquad (1)$$

where λ and λ_i are Lagrange multipliers and Q_i possible additional constraints (e.g., deformation) left out in the present Rapid Communication.

In Eq. (1), $\hat{H}(\rho)$ is the effective Hamiltonian defined as a functional of the one-body density ρ

$$\hat{H}(\rho) = \hat{K} + \hat{V}(\rho), \qquad (2)$$

containing a kinetic term $\hat{K}$ and a two-body density-dependent interaction term $\hat{V}(\rho)$ including the Coulomb potential. One-body and two-body center-of-mass corrections are implicit.

The trial wave functions $|\Psi\rangle$ appearing in Eq. (1), that describes nuclear stationary states, are expressed as linear combinations

$$|\Psi\rangle = \sum_{\alpha_\pi\alpha_\nu} A_{\alpha_\pi\alpha_\nu}|\phi_{\alpha_\pi}\phi_{\alpha_\nu}\rangle \qquad (3)$$

of direct products

$$|\phi_{\alpha_\pi}\phi_{\alpha_\nu}\rangle = |\phi_{\alpha_\pi}\rangle \otimes |\phi_{\alpha_\nu}\rangle \qquad (4)$$

of proton and neutron Slater determinants, $|\phi_{\alpha_\pi}\rangle$ and $|\phi_{\alpha_\nu}\rangle$ respectively, containing *a priori* any multiple p-h excitations that respect conserved quantum numbers. The one-body density ρ entering the effective Hamiltonian $\hat{H}(\rho)$ is the correlated one, $\rho = \langle\Psi|\hat{\rho}|\Psi\rangle$.

A variational principle applied to $\mathcal{F}(\rho)$ allows to determine both the mixing coefficients of the wave function and the optimal single-particle orbitals consistently with the correlations. The minimization of $\mathcal{F}(\rho)$ with respect to the $A_{\alpha_\pi\alpha_\nu}$ leads to a nonlinear secular equation equivalent to a diagonalization problem of a Hamiltonian matrix $\mathcal{H}$ in the multiconfigurational space,

$$\sum_{\alpha'_\pi\alpha'_\nu} \mathcal{H}_{\alpha_\pi\alpha_\nu,\alpha'_\pi\alpha'_\nu} A_{\alpha'_\pi\alpha'_\nu} = \lambda A_{\alpha_\pi\alpha_\nu}. \qquad (5)$$

The matrix $\mathcal{H}$ contains contributions of both the Hamiltonian $\hat{H}(\rho)$ and rearrangement terms $\mathcal{R}$ that come from the density dependence of the interaction.

The minimization of $\mathcal{F}(\rho)$ with respect to the single-particle orbitals leads to inhomogeneous Hartree-Fock (HF) equations,

which depend on correlations contained in $|\Psi\rangle$,

$$[h(\rho,\sigma),\rho] = G(\sigma), \tag{6}$$

where the irreducible (connected) two-body correlation matrix is given by

$$\sigma_{ij,kl} = \langle\Psi|a_i^+ a_k^+ a_l a_j|\Psi\rangle - \rho_{ji}\rho_{lk} + \rho_{jk}\rho_{li}. \tag{7}$$

In Eq. (6), $h(\rho,\sigma)$ is the one-body mean-field Hamiltonian built with the one-body density ρ and the connected part σ:

$$h_{ij}(\rho,\sigma) = \langle i|K|j\rangle + \Gamma_{ij}(\rho) + \partial\Gamma_{ij}(\rho) + \partial\Gamma_{ij}(\sigma). \tag{8}$$

Explicit expressions for the Hamiltonian matrix $\mathcal{H}$, the source term $G(\sigma)$, and for the fields $\Gamma_{ij}(\rho)$, $\partial\Gamma_{ij}(\rho)$ and $\partial\Gamma_{ij}(\sigma)$ are given in Refs. [17,18].

A fully self-consistent solution is obtained by solving simultaneously Eqs. (5)–(6). The only parameters of the model are those of the Gogny interaction. Analogous methods are well known in various fields of physics, as atomic physics or quantum chemistry [25,26]. They provide a very accurate description of the spectroscopy.

The present work has been performed in the same numerical framework as in Ref. [18]. In particular, even though the formalism has been developed in axial symmetry, the *m*p-*m*h CM calculations have been performed at the spherical point in order to generate correlated solutions with a good total angular momentum. Axial and spherical descriptions coincide for $\langle Q_i\rangle = 0$. Thus, the found eigenfunctions become laboratory solutions rather than intrinsic frame solutions. In this work the CM has been restricted to the *sd*-shell, including all possible configurations and only the first equation (5) has been considered. The fully self-consistent solution is beyond the scope of this paper. Then, the HF single-particle orbitals have been used to solve Eq. (5). Besides, the single-particle orbitals have been expanded on an axial harmonic oscillator basis with eleven major shells ensuring convergence. Finally, in order to quantify the accuracy of the results, the average difference $\langle x\rangle$ and the standard deviation $\sigma(x)$ of a given observable x are considered,

$$\langle x\rangle = \frac{1}{N_x}\sum_{i=1}^{N_x}|x_i| \quad \text{and} \quad \sigma(x) = \sqrt{\langle x^2\rangle - \langle x\rangle^2}.$$

Ground- and excited-state energies. We first discuss the binding energy (BE) behavior for the Ne, Mg, Si, S, and Ar nuclei. Including nuclear long-range correlations in a beyond MF approach is expected to wash out the structures displayed by the BE and dictated by shell effects [3,27]. On Fig. 1, the differences ΔBE from experimental BE [28], calculated in the spherical HF and *m*p-*m*h CM approximations, are presented for all selected isotopes. No data is available for ^{28}Ar. The quantity ΔBE is found essentially constant with an average difference $\langle\Delta\text{BE}\rangle = 8.532$ MeV in the *m*p-*m*h CM approach. In the HF case, it is equal to 3.352 MeV. These large values of ΔBE are expected. Indeed, the D1S Gogny force has been fitted in order to reproduce experimental masses of a few doubly magic nuclei at the restricted HF approximation [29]. Besides, the *m*p-*m*h CM approach provides a non-negligible amount of correlations even in doubly magic nuclei, which

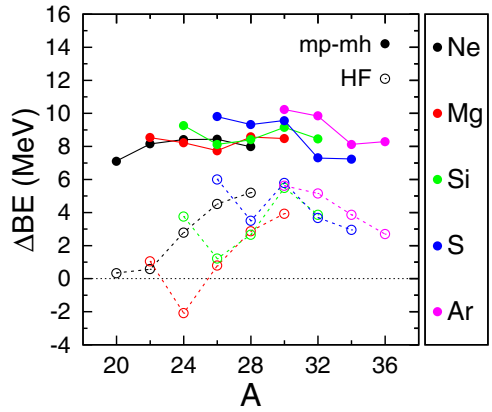

FIG. 1. (Color online) Difference to the experimental values of theoretical BE (in MeV) calculated at the HF and the *m*p-*m*h CM approximations.

explains the larger overbinding $\langle\Delta\text{BE}\rangle$. At the HF level, strong variations are found along isotopic chains. On the contrary, a very flat behavior is obtained when using the *m*p-*m*h CM approach. The most striking feature concerns the standard deviations $\sigma(\Delta\text{BE})$, equal to 0.824 MeV in the *m*p-*m*h CM approach and 1.727 MeV in the HF approximation. The treatment of the nuclear long-range correlations reduces by itself the dispersion of BE in a significant way, without any change in the effective interaction. The results obtained from HFB (spherical or deformed) and 5DCH calculations [3] using the same effective interaction for ΔBE exhibit similar behavior as the spherical HF ones, presented in Fig. 1.

From the BE, we have deduced the two-neutron S_{2n} and the two-proton S_{2p} separation energies. The differences ΔS_{2n} (a) and ΔS_{2p} (b) between theory and experiment [28] are plotted on Fig. 2. The theoretical results are deduced at both HF and *m*p-*m*h CM levels. As the *m*p-*m*h CM calculations have been restricted to nuclei with $8 < (Z,N) < 20$, the S_{2n} of $N = 10$ isotones as well as the S_{2p} of Ne isotopes have not been calculated. As seen from Fig. 2, the *m*p-*m*h CM S_{2n} and S_{2p} are found in a much better agreement with experiment than the HF ones due to the low standard deviation $\sigma(\Delta\text{BE})$. Concerning the S_{2n}, $\langle\Delta S_{2n}\rangle$ is equal to 0.613 MeV

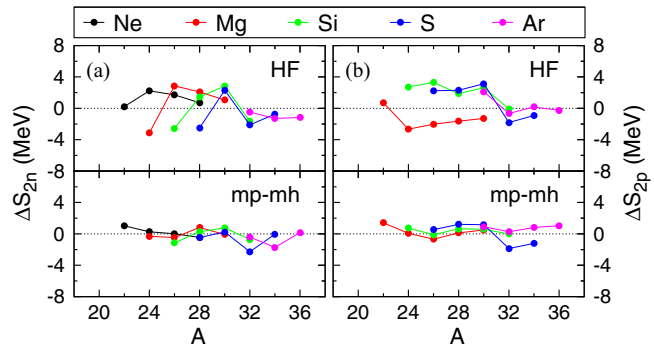

FIG. 2. (Color online) Differences ΔS_{2n} (a) and ΔS_{2p} (b) between experiment and theory calculated at the HF and *m*p-*m*h CM approximations (in MeV).

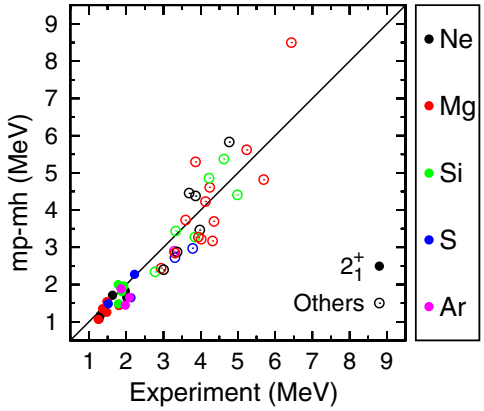

FIG. 3. (Color online) Comparison of experimental and theoretical excitation energies E^* (in MeV).

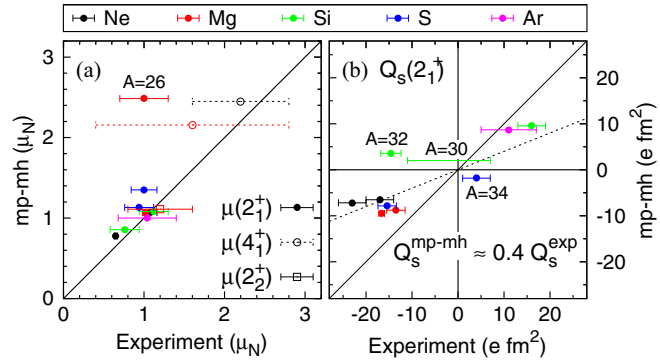

FIG. 4. (Color online) Comparison of experimental and theoretical (a) magnetic moments μ (in μ_N unit) and (b) quadrupole spectroscopic moments Q_s (in $e$fm^2).

and $\sigma(\Delta S_{2n})$ to 0.587 MeV with the mp-mh CM approach. In the HF case, the corresponding values are 1.741 MeV and 0.866 MeV. Concerning the S_{2p}, the values are found similar to the S_{2n} ones, 0.732 MeV and 0.504 MeV with the mp-mh CM approach, 1.711 MeV and 1.011 MeV in the HF case. As a consequence, the mp-mh CM approach is able to reproduce with a good accuracy the detailed experimental structures of the evolution of two-nucleon separation energy. In agreement with experiment, the mp-mh CM predicts that three isotopes (^{26}S, ^{28}Ar, and ^{30}Ar) are not bound using S_{2p} criteria. Consequently, they have been excluded in the following.

The analysis of the excited spectra focuses on the 0_2^+, 1_1^+, 2_1^+, 2_2^+, 3_1^+, 3_2^+, and 4_1^+ low-lying states known experimentally [30–36]. As mentioned in the Introduction, the CM occurs only in the *sd* shell. Hence, all states with an experimental excitation energy E^* at least lower by 1 MeV than the first experimental negative parity state have been kept. The results are shown in Fig. 3. A global shift of ∼2.5 MeV was obtained on the spectrum of ^{30}Si linked to uncontrolled $T = 0$ properties of the D1S Gogny force [18]. The same pathology is found here for its mirror nucleus ^{30}S and therefore they have been removed from Fig. 3. In total, our analysis is based on 48 excited states.

Quite satisfactory results are obtained for all isotopic chains. Indeed, $\langle \Delta E^* \rangle = 464$ keV and $\sigma(\Delta E^*) = 397$ keV (ΔE^* denotes the difference from experiment). For the 2_1^+ states, the agreement is even better, with $\langle \Delta E^*(2_1^+) \rangle = 196$ keV and $\sigma[\Delta E^*(2_1^+)] = 168$ keV. A previous study [37] using the same interaction has pointed out that quadrupole collective models are able to describe 2_1^+ states only qualitatively in these mass regions. The mp-mh CM approach is expected to systematically improve the description of 2_1^+ states in light- and medium-mass nuclei.

Magnetic dipole and electric quadrupole properties. The calculation of overlap functions as magnetic moments μ, spectroscopic quadrupole moments Q_s, $B(M1)$ and $B(E2)$ reduced transition probabilities is a stringent test of the magnetic dipole and electric quadrupole correlation content of the mp-mh CM wave functions. In Fig. 4(a) a comparison between experimental and theoretical μ is plotted (in μ_N unit). Almost all predicted $\mu(2_1^+)$ values are in excellent agreement with experimental data. The situation is unclear only for the ^{26}Mg isotope. Our prediction is compatible with the old experimental value (2.6 μ_N) that has been later reevaluated [1.0*(3)* μ_N] [33–35]. Our calculation reproduces well the only existing $\mu(2_2^+)$ data (^{24}Mg). For the 4_1^+ states, the calculated values are within the experimental error bars. However, as the error bars are large, it is still not possible to conclude on the accuracy of the theoretical predictions for these states.

In Fig. 4(b), experimental and theoretical $Q_s(2_1^+)$are compared. The theory systematically underestimates experimental values. A linear fit provides a slope of ∼0.4. This behavior was expected since a limited valence space is used in the present calculations, which do not allow us to fully describe the quadrupole collectivity properties of these states. This point will be discussed further in more detail. An interesting feature is that, in the large majority of cases, the experimental sign of $Q_s(2_1^+)$ is obtained. Only the theoretical signs for ^{32}Si and ^{34}S differ from experiment. Concerning the ^{30}Si isotope, two different data are reported in Ref. [30]: $-5(6)$ and $+1(6)$ $e$fm^2. Our calculation provides a value of $+2$ $e$fm^2, compatible with the second experimental data.

To complete our study on magnetic dipole and electric quadrupole collectivities, we have investigated the transition probabilities, 13 $B(M1)$ and 51 $B(E2)$. The experimental and theoretical $B(M1)$ are presented in Table I. An overall good agreement is obtained. The orders of magnitude, that range from 10^{-6} to 10^{-1} in Weisskopf units, are systematically reproduced by our calculations. This emphasizes once more the ability of the mp-mh CM approach in reproducing the experimental trends. The worst discrepancy corresponds to a factor ∼5 for the $1_1^+ \rightarrow 2_1^+$ transition in ^{30}Si.

The whole set of experimental and theoretical values for $B(E2)$ is displayed in Fig. 5. One observes that the experimental $B(E2)$ values are systematically underestimated by the theory. They are distributed along a line with a slope of ∼0.25. As for the Q_s, this behavior is expected since the CM is used in a limited valence space. A similar behavior is seen in SM studies [16,23]: if no effective charge is used, the $B(E2)$ are reproduced within a ∼0.3 factor. The answer proposed by the mp-mh CM is to introduce at least part of the missing collectivity by determining the optimized orbitals [see Eq. (6)].

TABLE I. Comparison between experimental and theoretical $B(M1)$ transition probabilities (in Weisskopf units).

Nucleus	Transition	Experiment	mp-mh
^{24}Mg	$2_2^+ \to 2_1^+$	9×10^{-6} (8)	7×10^{-6}
	$3_1^+ \to 2_1^+$	2.1×10^{-5} (1.1)	4.6×10^{-5}
	$3_1^+ \to 2_2^+$	3.5×10^{-4} (1.7)	2.5×10^{-4}
^{26}Mg	$2_2^+ \to 2_1^+$	0.097 (12)	0.066
	$3_1^+ \to 2_1^+$	0.00102 (15)	0.00375
	$3_1^+ \to 2_2^+$	0.0159 (23)	0.0260
	$3_2^+ \to 2_1^+$	0.0067 (14)	0.0041
	$3_2^+ \to 2_2^+$	0.032 (7)	0.055
^{26}Si	$2_2^+ \to 2_1^+$	0.10 (3)	0.07
^{30}Si	$2_2^+ \to 2_1^+$	0.09 (3)	0.19
	$1_1^+ \to 2_1^+$	0.091 (23)	0.457
^{34}S	$2_2^+ \to 2_1^+$	0.052 (3)	0.059
^{34}Ar	$2_2^+ \to 2_1^+$	0.058 (12)	0.030

A complementary analysis of the 22 $B(E2,2_1^+ \to 0_1^+)$ have been performed in terms of isotopic and isotonic chains. Examples are presented in Fig. 6 for the Ne and S isotopes as well as for the $N = 14$ and $N = 18$ isotones. The mp-mh CM reproduces in a very satisfactory way the experimental trends. The analysis of the mp-mh CM wave functions reveals that, in ^{28}S and ^{34}S, the 0_1^+ and 2_1^+ states have similar structures dominated by the 0p-0h component. Since ^{30}S and ^{32}S are closed subshell nuclei, the 0_1^+ and 2_1^+ states exhibit very different structures, characterized by the absence of a 0p-0h component in the 2_1^+ states whose major configuration is a 1p-1h excitation. The weight of the main component is typically ∼60% in the 0_1^+ states and ∼45% in the 2_1^+ states, producing a too flat $B(E2)$ behavior as compared to experiment. Concerning the Ne isotopes, the 0_1^+ and 2_1^+ states display similar structures with a 0p-0h main component. However, the heaviest ones are more closed than the lightest ones, in agreement with the $B(E2)$ decreasing experimental trend. The weight of the 0p-0h component is ∼47% in the 0_1^+ state and ∼37% in the 2_1^+ state for ^{20}Ne whereas it reaches ∼87% and ∼85%, respectively, for ^{28}Ne.

Discussion. To conclude the analysis, we discuss how to account for the quadrupole collectivity beyond the *sd* shell. A global factor F applied to all values (see Fig. 6) cannot account accurately for the electric quadrupole collectivity. For example, in the case of S isotopes, even if predictions are

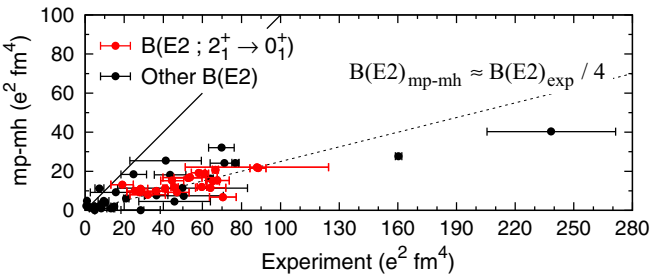

FIG. 5. (Color online) $B(E2)$ reduced transition probabilities (in e^2 fm^4). The $2_1^+ \to 0_1^+$ transitions appear in red.

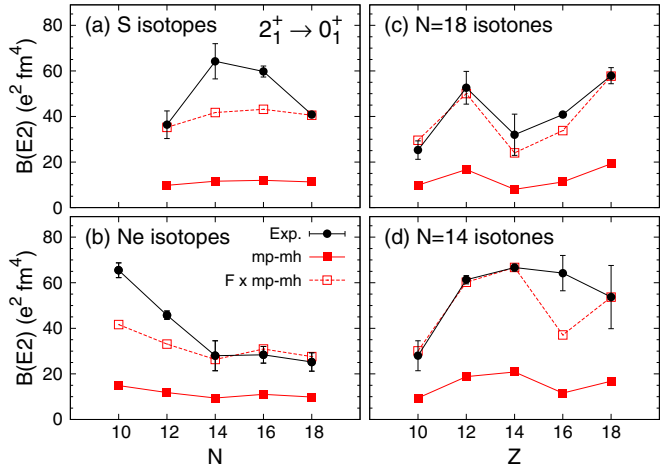

FIG. 6. (Color online) Examples of reduced transition probabilities $B(E2,2_1^+ \to 0_1^+)$ for isotopic (left) and isotonic (right) chains. Theoretical (experimental) values are in red (black).

multiplied by $F = 3.6$ in order to match with the experimental values of ^{28}S and ^{34}S, a non-negligible lack of collectivity is still present in ^{30}S and ^{32}S. An inspection of the ^{32}S axial potential energy curves (PECs) shows that a second minimum develops at a large value of the axial deformation parameter β, around 1.2. The minimum is produced by the opening of a deformed gap due to the $1f_{7/2}$ shell. In the ^{30}S case, an inflection of the PECs is observed around the same deformation. These theoretical results are in agreement with many other studies. Besides, the existence of superdeformed states as well as α clustering are expected at a similar deformation [38–40] in ^{32}S and in the neighbor nuclei [41]. The prolate softness of these PECs may modify partly the collective structure of the 2_1^+ in both ^{30}S and ^{32}S. For the Ne isotopes, applying a factor $F = 2.8$ to the theoretical $B(E2)$ leads to the same conclusion. In the lightest Ne isotopes, a different neutron collectivity is expected to induce an increase of the quadrupole softness of the PEC.

In order to understand the lack of electric quadrupole collectivity, a quantitative analysis based on the axial deformation properties of the HF PEC has been performed with the D1S interaction and presented here for the Ne isotopes. At various axial deformations β, we have calculated the neutron and proton occupation probabilities $p_i^{\nu,\pi}$ of spherical orbitals i from the filled deformed orbitals α defined as

$$p_i(\beta) = \sum_{\alpha=1}^{N} \chi_{i\alpha}^2(\beta),$$

where $\chi_{i\alpha}$ is the overlap between the deformed and spherical HF orbitals. As an illustration, the axial PECs of ^{20,24,28}Ne are displayed in Fig. 7 (left panel) as well as the associated quantity

$$P_{\text{shell}}^{\nu,\pi}(\beta) = \sum_{i \in \text{shell}} \left[p_i^{\nu,\pi}(\beta) - p_i^{\nu,\pi}(0) \right],$$

for each major shell (right panel). The PECs are found to be soft against β. For the lightest isotopes ($^{20-24}$Ne), the

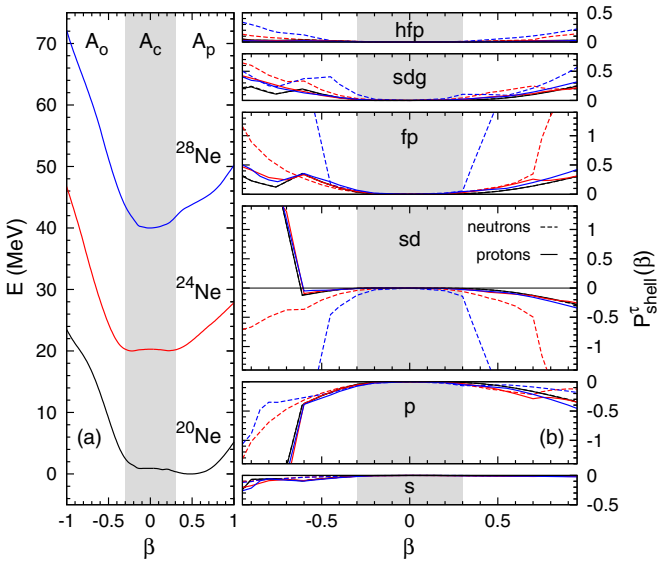

FIG. 7. (Color online) Axial PEC (left) and $P^{\tau}_{\rm shell}(\beta)$ (right) for Ne isotopes.

absolute minima are either prolate (^{20,22}Ne) or oblate (^{24}Ne). They are found spherical in ^{26,28}Ne. The $P^{\pi}_{\rm shell}(\beta)$ exhibit similar behaviors according to β indicating that the proton quadrupole collectivity is expected to be analogous for all isotopes. In the central gray area A_c with $\beta \in [-0.3,0.3]$, the coupling between the proton sd shell and the others is negligible as $P^{\pi}_{\rm shell}(\beta) \approx 0$. One notes that the A_c area, characterizing essentially the $0\hbar\omega$ configurations, does not match well with the PEC patterns. In the lightest isotopes, the prolate minima are clearly outside of A_c. In the A_o and A_p areas where $2\hbar\omega$ configurations exist, the couplings appear, in particular between the p and fp shells, the sd and fp shells or the p and sd shells. For neutrons, the behavior of $P^{\nu}_{\rm shell}(\beta)$ depends on the isotope. In ^{20,22}Ne, the evolution of $P^{\nu}_{\rm shell}(\beta)$ is similar to the one of $P^{\pi}_{\rm shell}(\beta)$. For $^{24-28}$Ne, the couplings between shells are found larger and strong variations of $P^{\nu}_{\rm shell}(\beta)$ occur for smaller β values. The associated neutron quadrupole collectivity that decreases from ^{20}Ne to ^{28}Ne leads to a transition from deformed to spherical minima.

To conclude, the electric quadrupole collectivity of the mp-mh CM wave functions, tested in the $B(E2)$ calculation, are expected to be corrected if the $2\hbar\omega$ excitations, corresponding to $(1\text{p-}1\text{h})^{\pi,\nu}$, $(2\text{p-}2\text{h})^{\pi,\pi\nu}$ configurations built with other shells than simply the sd shell are introduced, thus accounting for core polarization. The contributions of the neutrons to the $B(E2)$ comes mainly from proton-neutron couplings. As these couplings may differ in the various isotopes, this could explain the missing collectivity in the $B(E2)$ of ^{20}Ne and ^{22}Ne. Since the $M1$ strength is exhausted with $0\hbar\omega$ configurations, the μ and $B(M1)$ are essentially well described within the present limited valence space. This is a clear indication that the D1S Gogny force has good magnetic properties in the sd shell. Concerning other observables discussed in the present work, the additional $2\hbar\omega$ configurations are expected to produce an overall increase of the binding energies. Moreover, they correspond to relatively high-energy configurations and they are expected to add similar amount of correlations in ground and excited states. Thus, the excitation energies are expected to stay rather stable when introducing these additional configurations.

Conclusion. In the present study, a coherent and promising description of many observables is highlighted in even-even sd-shell nuclei, using the mp-mh configuration mixing and the D1S Gogny interaction. The standard deviations σ concerning binding energies, two-nucleon separation energies and excitation energies are very good, considering that the Gogny interaction was not derived *a priori* to be used with such a general approach, which includes all kinds of nuclear long-range correlations. The results associated with magnetic dipole moments, spectroscopic quadrupole moments as well as $B(M1)$ and $B(E2)$ reduced transition probabilities are very encouraging. Indeed, the experimental trends are systematically obtained. Only a lack of electric quadrupole collectivity is observed, resulting from a limited valence space. Work is in progress to improve the quadrupole correlation description by completing the mp-mh configuration mixing wave functions with $2\hbar\omega$ configurations.

N.P. acknowledges D. Gogny for valuable comments and suggestions about this work as well as F. Nowacki for his critical and helpful reading of the manuscript.

[1] P. Ring and P. Schuck, *The Nuclear Many-Body Problem* (Springer-Verlag, New York, 1980).
[2] M. Bender, P.-H. Heenen, and P.-G. Reinhard, Rev. Mod. Phys. **75**, 121 (2003).
[3] J.-P. Delaroche, M. Girod, J. Libert, H. Goutte, S. Hilaire, S. Péru, N. Pillet, and G. F. Bertsch, Phys. Rev. C **81**, 014303 (2010).
[4] J. L. Egido and P. Ring, Nucl. Phys. A **383**, 189 (1982).
[5] M. Anguiano, J. L. Egido, and L. M. Robledo, Nucl. Phys. A **696**, 467 (2001).
[6] J. P. Blaizot and D. Gogny, Nucl. Phys. A **284**, 429 (1977).
[7] E. Khan and Nguyen Van Giai, Phys. Lett. B **472**, 253 (2000).
[8] T. Nakatsukasa, K. Matsuyanagi, I. Hamamoto, and W. Nazarewicz, Nucl. Phys. A **573**, 333 (1994).
[9] S. Péru and H. Goutte, Phys. Rev. C **77**, 044313 (2008).
[10] D. Gambacurta, M. Grasso, and F. Catara, Phys. Rev. C **81**, 054312 (2010).
[11] J. Dukelsky and P. Schuck, Phys. Lett. B **387**, 233 (1996).
[12] N. Pillet, P. Quentin, and J. Libert, Nucl. Phys. A **697**, 141 (2002).
[13] J. Le Bloas, L. Bonneau, P. Quentin, J. Bartel, and D. D. Strottman, Phys. Rev. C **86**, 034332 (2012).
[14] E. Caurier, G. Martínez-Pinedo, F. Nowacki, A. Poves, and A. P. Zuker, Rev. Mod. Phys. **77**, 427 (2005).
[15] T. Otsuka, M. Honma, T. Mizusaki, N. Shimizu, and Y. Utsuno, Prog. Part. Nucl. Phys. **47**, 319 (2001).
[16] B. A. Brown and B. H. Wildenthal, Annu. Rev. Nucl. Part. Sci. **38**, 29 (1988).

[17] N. Pillet, J.-F. Berger, and E. Caurier, Phys. Rev. C **78**, 024305 (2008).
[18] N. Pillet, V. G. Zelevinsky, M. Dupuis, J.-F. Berger, and J.-M. Daugas, Phys. Rev. C **85**, 044315 (2012).
[19] A. Bohr and B. R. Mottelson, *Nuclear Structure* (Benjamin, New York, 1975), Vol. II.
[20] I. Hamamoto, J. Sagawa, and X. Z. Zhang, Nucl. Phys. A **626**, 669 (1997).
[21] B. A. Brown and B. H. Wildenthal, Nucl. Phys. A **474**, 290 (1987).
[22] G. Martínez-Pinedo, A. Poves, L. M. Robledo, E. Caurier, F. Nowacki, J. Retamosa, and A. Zuker, Phys. Rev. C **54**, R2150 (1996).
[23] W. A. Richter, S. Mkhize, and B. A. Brown, Phys. Rev. C **78**, 064302 (2008).
[24] J.-F. Berger, M. Girod, and D. Gogny, Comput. Phys. Commun. **63**, 365 (1991).
[25] C. Froese Fischer, Comput. Phys. Commun. **1**, 151 (1969); J. C. Morrison and C. Froese Fischer, Phys. Rev. A **35**, 2429 (1987).
[26] D. L. Yeager and P. Jorgensen, J. Chem. Phys. **71**, 755 (1979); H. J. Werner and W. Meyer, *ibid.* **74**, 5802 (1981).
[27] A. Arcones and G. F. Bertsch, Phys. Rev. Lett. **108**, 151101 (2012).
[28] M. Wang, G. Audi, A. H. Wapstra, F. G. Kondev, M. MacCormick, X. Xu, and B. Pfeiffer, Chin. Phys. C **36**, 1603 (2012).
[29] D. Gogny, in *Proceedings of the International Conference on Nuclear Self-Consistent Fields, Trieste*, edited by G. Ripka and M. Porneuf (North-Holland, Amsterdam, 1975), p. 333.
[30] National Nuclear Data Center, Evaluated Nuclear Structure Data File, http://www.nndc.bnl.gov/ensdf/.
[31] S. Raman, C. H. Malarkey, W. T. Milner, C. W. Nestor, Jr., and P. H. Stelson, At. Data Nucl. Data Tables **36**, 1 (1987).
[32] Y. Togano *et al.*, Phys. Rev. Lett. **108**, 222501 (2012).
[33] J. L. Eberhardt, R. E. Horstman, H. W. Heeman, and G. Van Middelkoop, Nucl. Phys. A **229**, 162 (1974).
[34] P. C. Zalm, A. Holthuizen, J. A. G. De Raedt, and G. Van Middelkoop, Hyperfine Interact. **5**, 347 (1978).
[35] K. H. Speidel, G. J. Kumbartzki, W. Knauer, M. Knopp, V. Mertens, P. N. Tandon, J. Gerber, and R. M. Freeman, Phys. Lett. B **102**, 6 (1981).
[36] J. Gibelin *et al.*, Phys. Rev. C **75**, 057306 (2007).
[37] G. F. Bertsch, M. Girod, S. Hilaire, J.-P. Delaroche, H. Goutte, and S. Péru, Phys. Rev. Lett. **99**, 032502 (2007).
[38] T. Ichikawa, Y. Kanada-En'yo, and P. Möller, Phys. Rev. C **83**, 054319 (2011).
[39] T. Inakura, S. Mizutori, M. Yamagami, and K. Matsuyanagi, Nucl. Phys. A **710**, 261 (2002).
[40] R. R. Rodríguez-Guzmán, J. L. Egido, and L. M. Robledo, Phys. Rev. C **62**, 054308 (2000).
[41] D. G. Jenkins *et al.*, Phys. Rev. C **86**, 064308 (2012).